scientific reports

Check for updates

OPEN

Fractal charge distribution on closed surfaces generated by finite element triangles

Haotian Chen[1], B. Da[3]✉ & Z. J. Ding[1,2]✉

A finite element method is employed to calculate the spatial electric potential generated by isolated conductors, where free charges distribute themselves in accordance with classical electrostatics. Remarkably, a novel fractal structure emerges in the surface charge distribution on curved geometries such as spheres and tori. This fractal behavior is distinct from that of the finite element area distribution, highlighting a fundamental difference: the fractal patterns that arise under physical constraints—specifically, Coulomb's law in this study—differ significantly from those produced by purely geometrical operations.

Keywords Fractal, Sphere, Triangle, Charge density distribution

Fractals, geometric structures that display self-similarity across scales, have emerged as a pervasive and intriguing phenomenon in both mathematics and the natural world[1]. Mathematically, fractals are typically defined through recursive or iterative processes that generate intricate patterns with non-integer dimensions, known as fractal dimensions. Mandelbrot introduced several two-dimensional iconic fractal sets, such as the Mandelbrot set and Julia sets, which exhibit complex behavior under iteration[2,3]. With advances in computational techniques, the exploration of high-dimensional fractals and their applications, ranging from image compression and data analysis to the modeling of complex physical systems[4–7], has significantly expanded.

A classic example of a fractal is the Sierpiński gasket, formed by recursively subdividing and removing smaller triangles from an initial equilateral triangle. Variants inspired by this process such as the Sierpiński carpet and Sierpiński tetrahedron, extend this idea to other geometric contexts. Similar iterative subdivision processes can also be applied to Platonic solids, resulting in polyhedral approximations of spheres[8]. These polyhedral spheres exhibit self-similar patterns in their triangle areas[9]. In this study, such self-repeating, scale-dependent patterns are referred to as fractal patterns, as they closely resemble the characteristics of mathematical fractals. These structures provide a geometric foundation for studying fractality on spheres, and have been further utilized to generate fractal patterns on two-dimensional surfaces[10].

According to classical electrostatics, an isolated conductor in equilibrium must be an equipotential body, with all excess charge residing on its surface according to Gauss's law. While the surface charge density is analytically known for highly symmetric cases[11–13], such as an ideal sphere, but in most geometries, an exact expression is unavailable. Numerical methods, particularly the finite element method, offer a practical solution for approximating charge distributions and computing spatial electric potentials and electric fields.

The primary aim of this study is to investigate surface charge distributions on various geometrical conductors, a cube, a sphere, and a torus, using triangular finite element mesh. To approach ideal smooth surfaces, we iteratively subdivide the triangular mesh, analogous to the recursive refinement seen in Sierpiński-like fractals[9]. As the rank of subdivision increases, the calculated electric potential more closely approximates theoretical expectations, validating the approach.

However, a surprising observation emerges. The charge distribution exhibits a distinct fractal pattern, one that differs significantly from the triangle area distribution. This difference stems from the dual influence of geometric and physical constraints. While the area distribution is purely geometry, the charge distribution must also obey electrostatic laws. Thus, the fractal nature of the charge distribution represents a novel class of physically constrained fractals.

[1]Department of Physics, University of Science and Technology of China, Hefei 230026, Anhui, People's Republic of China. [2]Hefei National Laboratory for Physical Science at Microscale, University of Science and Technology of China, Hefei 230026, Anhui, People's Republic of China. [3]Center for Basic Research On Materials, National Institute for Materials Science, Tsukuba, Ibaraki 305-0044, Japan. ✉email: DA.Bo@nims.go.jp; zjding@ustc.edu.cn

Theoretical model

Triangle subdivision

We employ a finite element method that approximates the surface of a solid conductor with a polyhedral mesh composed entirely of triangles, such that all vertices of this mesh are constrained to lie on the surface of the conductor. To improve the approximation of the surface geometry and increase the resolution of the charge distribution, the triangular faces of the initial polyhedron are recursively subdivided. We define the initial polyhedron as the zeroth-rank polyhedron. After n subdivisions, we obtain the n th rank polyhedron. As $n \to \infty$, the polyhedral mesh converges to the true smooth closed surface of the conductor. Note that the n th rank polyhedron is totally decided by the initial polyhedron.

The subdivision scheme is illustrated in Fig. 1. Consider a triangle ΔABC on the surface mesh. During subdivision, we introduce three new points P_A, P_B and P_C on the plane of ΔABC. However, these points may not lie on the actual curved surface of the conductor. In this case, we project each point to the nearest location on the surface, obtaining P'_A, P'_B and P'_C, respectively. Therefore, we define a subdivision of a triangle on the surface to be from ΔABC to $\Delta AP'_BP'_C$, $\Delta BP'_CP'_A$, $\Delta CP'_AP'_B$ and $\Delta P'_AP'_BP'_C$.

Approximated electrostatic potential

Electrostatic potential is calculated by using Coulomb's potential

$$V(r) = k\frac{q}{r} \tag{1}$$

where k is Coulomb constant and set to unity for the sake of convenience, r is the distance from the charge q to the field position $\mathbf{r}$. To simplify the calculation, we assume that the surface charge density for one triangle face is a constant. Furthermore, we also assume that all of the charges are located on the centroid of the triangle; this assumption is obviously an approximation which is valid only at infinite rank. However, we still would like to consider to use this assumption for obtaining fractal structure served as a guidance to the result of accurate calculation in the following section. The electric potential of the i th triangle face is considered to be the potential on its centroid, which is calculated through

$$V_i = \sum_{j\neq i} \frac{q_j}{r_{ij}} + \frac{q_i}{r_{ii}} \tag{2}$$

where q_j is total charge on j th triangle face, r_{ij} is the distance from the centroid of i th triangle to the centroid of j th triangle when $i \neq j$, and r_{ii} is the reduced distance which is used to represent the electric potential generated by i th triangle itself.

In this study, the reduced distance r_{ii} is defined as

$$\frac{1}{r_{ii}} = \frac{1}{d_{i1}} + \frac{1}{d_{i2}} + \frac{1}{d_{i3}} \tag{3}$$

where d_{i1}, d_{i2} and d_{i3} are the distances from the centroid of the i th triangle to its three vertices. The details of obtaining this expression are discussed in Appendix A.

When charges reach electrostatic equilibrium, all the triangles must in the same potential. Assuming the total charge is 1, we have linear equations

$$\begin{cases} \sum\limits_j \frac{1}{r_{ij}} q_j = V_s, \\ \sum\limits_j q_j = 1, \end{cases} \tag{4}$$

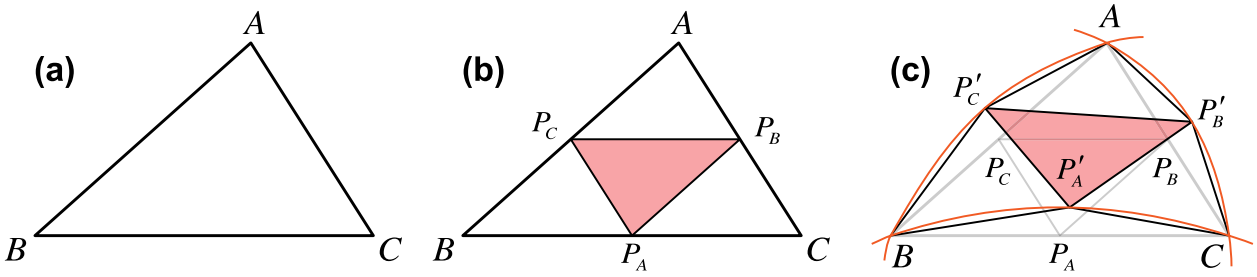

Fig. 1. The schematic diagram of subdividing a triangle on a surface: (**a**) an initial triangle, where $_A$, B and C are the vertices of the initial triangle lie on the modeled surface; (**b**) subdivided triangles, where P_A, P_B and P_C are the midpoints of BC, CA and AB, respectively; (**c**) subdividing scheme for the triangle on a surface, where P'_A, P'_B and P'_C are the positions lie on the surface and are closest to P_A, P_B and P_C, respectively.

for determination of charges distributed in each triangle and V_s, where V_s is the electrostatic potential of the conductor. Therefore, the boundary condition in this work corresponds to a Dirichlet boundary condition where the electric potential on the conductor surface is constant.

Analytical electrostatic potential

Analytical potential expression involves the integration to Eq. (1). Here we present a different but much simpler analytical expression than that given in Ref.[14]. Detailed formula derivation is discussed in Appendix B, here we present only an outline of our derivation procedure.

The analytical expression of the potential generated from any uniformly charged triangle in 3-dimensional Cartesian coordinate can be deduced from the potential of the origin, because translations and rotations preserve potential values. If the triangle is not parallel to the xOy-plane, we rotate its vertices around the origin with Rodrigues' rotation formula[15], so that after the rotation the plane equation of the triangle is $z = z_0$ for some constant z_0.

After the rotation, the integration of the potential is reduced in 2-dimensional coordinate. Let T be the rotated triangle and ΔABC be its projection on the xOy-plane. If the line $\overline{AB}$ does not go across the origin, its equation in the polar coordinate can be written as

$$\rho = \frac{1}{W} \sec(\theta - \phi) \tag{5}$$

where W and ϕ are constants depending on the coordinates of the points A and B. Assuming $W > 0$ for simplicity, then we have an intermediate integration

$$I(A,B) = \left(\frac{1}{W} \operatorname{arcsinh}\left(\frac{\tan(\theta - \phi)}{\sqrt{1 + z_0^2 W^2}} \right) + z_0 \arcsin\left(\frac{z_0 W \sin(\theta - \phi)}{\sqrt{1 + z_0^2 W^2}} \right) - |z_0|\,\theta \right) \Bigg|_{\theta=\alpha}^{\beta} \tag{6}$$

where α and β are the polar angles of the points A and B, respectively, and they must satisfy $\phi - \pi/2 < \alpha, \beta < \phi + \pi/2$. The sign of the sum $I(A,B) + I(B,C) + I(C,A)$ depends on the orientation of (A,B,C), then we have a final integration

$$I = |I(A,B) + I(B,C) + I(C,A)| \tag{7}$$

and the potential at origin generated by triangle T with charge area density σ is $V = \sigma I$.

The electric potential of the i th triangle face is also considered to be the potential on its centroid. Let c_{ij} be the integral of Eq. (7) at the centroid of the i th triangle generated from the j th triangle, then the linear system in Eq. (4) is modified as:

$$\begin{cases} \sum\limits_j c_{ij}\sigma_j = V_s, \\ \sum\limits_j S_j\sigma_j = 1, \end{cases} \tag{8}$$

where σ_j and S_j are the charge area density and triangle area of the j th triangle.

We have verified numerically that our integration expression, Eq. (7), procedures the same result as that given by Ref.[14] on the triangle with three vertices, $(0,0,z)$, $(x_2,0,z)$ and (x_3,y_3,z) on the grid constructed in region $0 \le z \le 1, 0 < x_2 \le 1, 0 < x_3 \le 2$ and $0 < y_3 \le 1$ with a step size of 0.01.

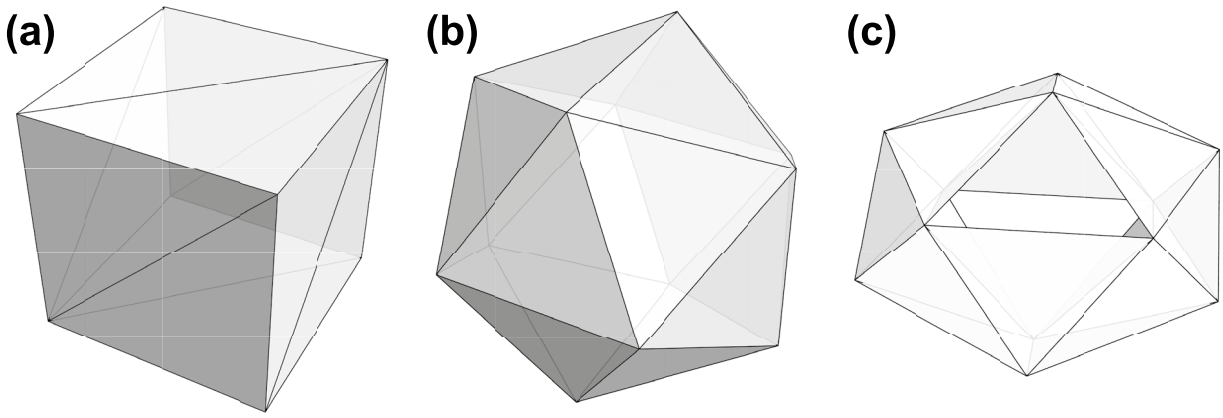

Fig. 2. The initial polyhedra of (**a**) cube, (**b**) sphere and (**c**) torus.

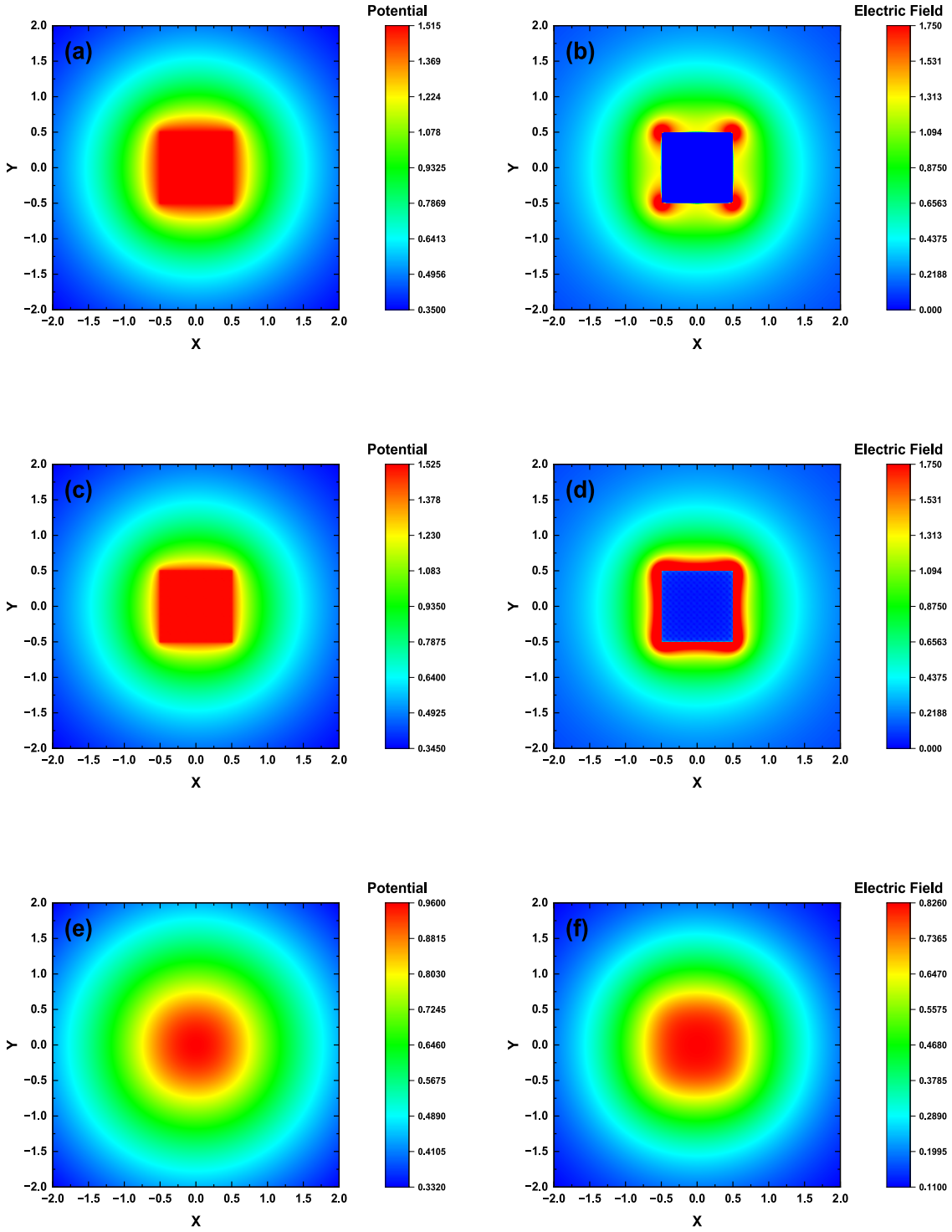

Fig. 3. The spatial electric potential (left column) and the electric field strength (right column) distributions for the 9th rank polyhedron of cube on the plane: (**a**), (**b**) $z = 0$; (c) $z = 1/2$; (**d**) $z = 0.499$; (**e**), (**f**) $z = 1$.

Results and discussions

We have considered charge distributed on a unit cube, a unit sphere and a torus with major radius $R = 1$ and minor radius $r = 1/3$. Their initial polyhedra are shown in Fig. 2. According to these, the charges and the charge densities for all the triangles on the surfaces of the polyhedra are at first calculated by Eq. (4) from the first rank to the ninth rank. Later we have also calculated the charge area densities by Eq. (8) from the first rank to the seventh rank. Equation (8) follows accurately physical law; however, the numerical calculation requires much more computational resource. Although Eq. (4) is an approximate and numerical solution, it can produce the

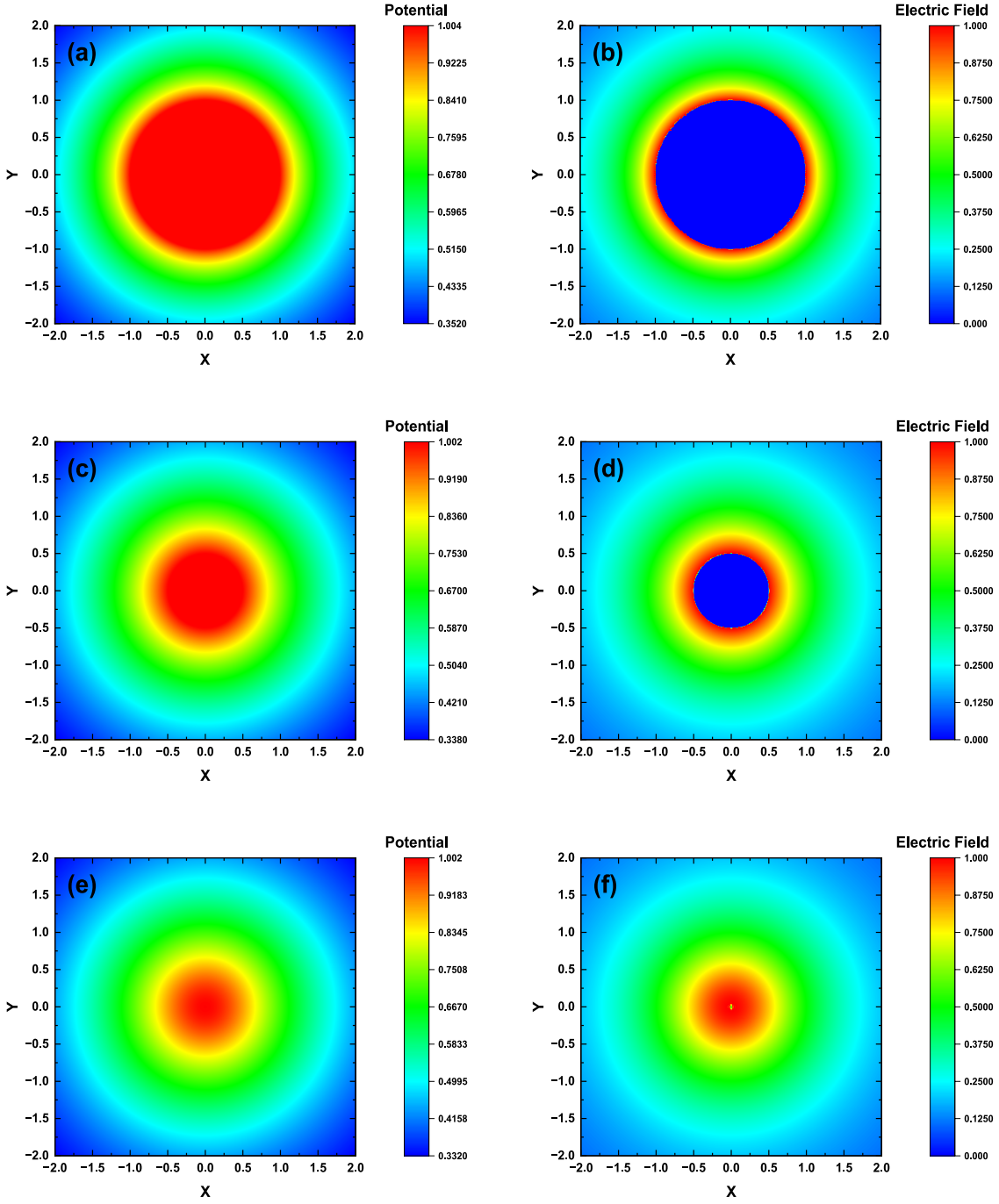

Fig. 4. The spatial electric potential (left column) and the electric field strength (right column) distributions for the 9th rank polyhedron of sphere on the plane: (**a**), (**b**) $z = 0$; (**c**), (**d**) $z = \sqrt{3}/2$; (**e**), (**f**) $z = 1$.

basic character of the 3D fractal structure at less computation cost. The two approaches are expected to agree each other at infinite rank.

Due to the physical quantity is generally a continuous variable, the fractal obtained here has an obvious character differing with other 2D/3D fractals that the intensity is continuously modulated. For the sake of convenience in the following content the triangle area distribution, charge distribution, the charge density distribution and constructed mathematical distribution are plot by coloring the triangles with a linear contour map between the blue (for the minimum value) and red (for the maximum value) according to the weight of a triangle (i.e., the triangle size), charge quantity, the charge density and the pure value, respectively.

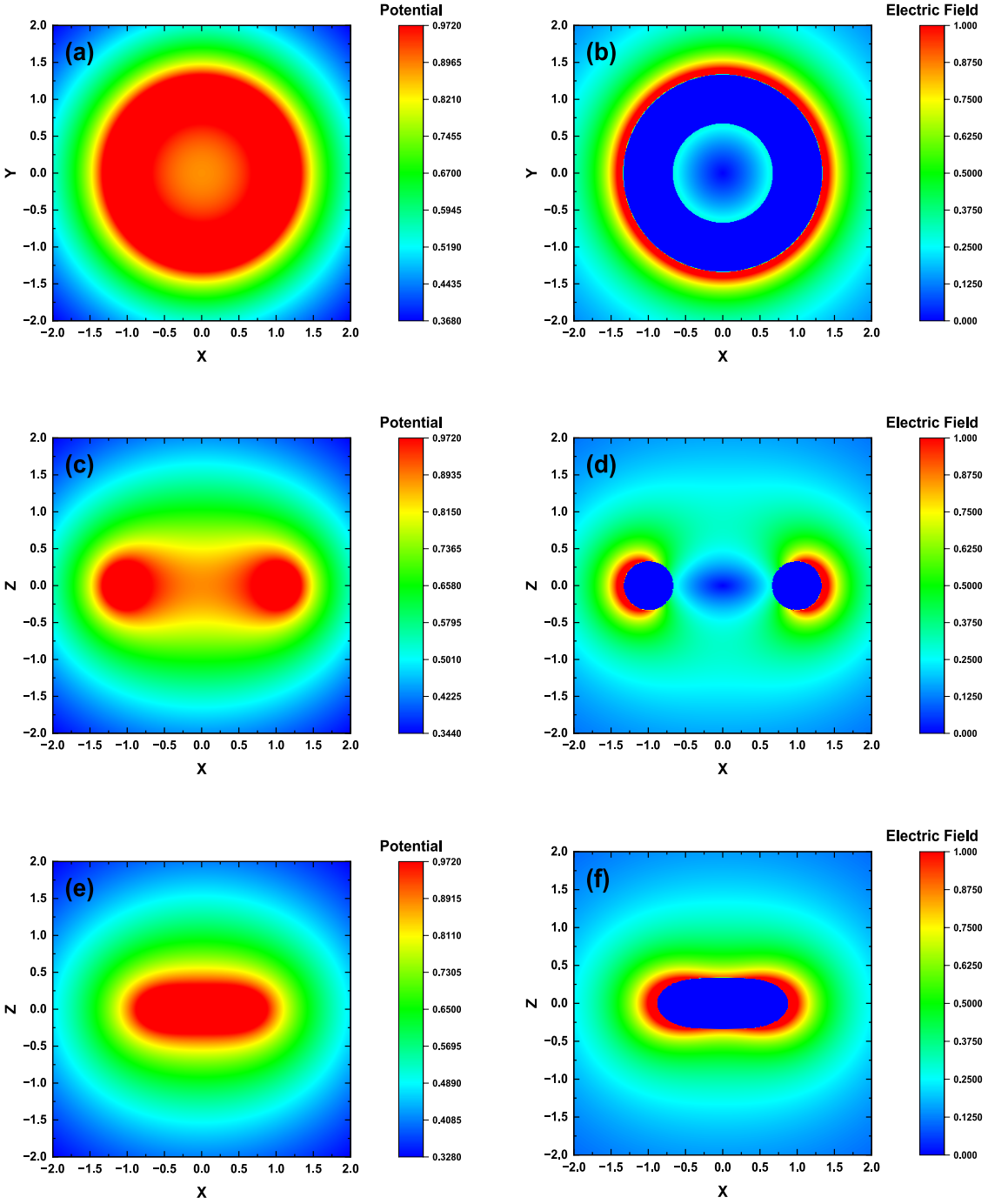

Fig. 5. The spatial electric potential (left column) and the electric field strength (right column) distributions for the 9th rank polyhedron of torus on the plane: (**a**), (**b**) $z = 0$; (**c**), (**d**) $y = 0$; (**e**), (**f**) $y = 1$.

Spatial potential and field distributions

After all q_j are obtained from Eq. (4), the electric potentials and the electric field strengths can be obtained from the equations,

$$V(\mathbf{r}) = \sum_j \frac{q_j}{|\mathbf{r} - \mathbf{r}_j|} \tag{9}$$

and

	Cube		Sphere		Torus	
rank	minimum	maximum	minimum	maximum	minimum	maximum
1	1.25×10^{-1}	1.25×10^{-1}	1.39×10^{-1}	1.65×10^{-1}	6.43×10^{-2}	2.03×10^{-1}
2	3.13×10^{-2}	3.13×10^{-2}	3.60×10^{-2}	4.57×10^{-2}	1.23×10^{-2}	6.18×10^{-2}
3	7.81×10^{-3}	7.81×10^{-3}	9.08×10^{-3}	1.17×10^{-2}	2.84×10^{-3}	1.69×10^{-2}
4	1.95×10^{-3}	1.95×10^{-3}	2.28×10^{-3}	2.95×10^{-3}	6.94×10^{-4}	4.33×10^{-3}
5	4.88×10^{-4}	4.88×10^{-4}	5.69×10^{-4}	7.40×10^{-4}	1.73×10^{-4}	1.09×10^{-3}
6	1.22×10^{-4}	1.22×10^{-4}	1.42×10^{-4}	1.85×10^{-4}	4.31×10^{-5}	2.73×10^{-4}
7	3.05×10^{-5}	3.05×10^{-5}	3.56×10^{-5}	4.63×10^{-5}	1.08×10^{-5}	6.82×10^{-5}
8	7.63×10^{-6}	7.63×10^{-6}	8.89×10^{-6}	1.16×10^{-5}	2.69×10^{-6}	1.70×10^{-5}
9	1.91×10^{-7}	1.91×10^{-7}	2.22×10^{-6}	2.89×10^{-6}	6.73×10^{-7}	4.26×10^{-6}

Table 1. The minimum and the maximum values of all triangle areas on the polyhedra of cube, sphere and torus.

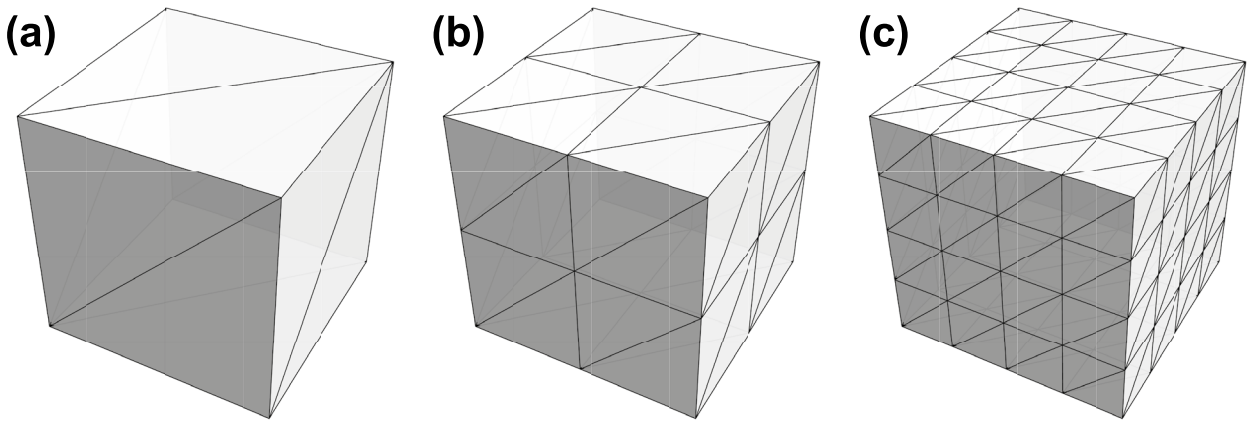

Fig. 6. The triangles and their edges on (**a**) 0th rank, (**b**) 1st rank and (**c**) 2nd rank of triangular cube surface.

$$|\mathbf{E}(\mathbf{r})| = \left| \sum_j q_j \frac{\mathbf{r} - \mathbf{r}_j}{|\mathbf{r} - \mathbf{r}_j|^3} \right| \tag{10}$$

where $\mathbf{r}_j$ is the position vector of the centroid of the j th triangle. The calculated spatial distributions of the electric potentials and the field strengths on some specific planes for each polyhedron considered at the highest rank (i.e. ninth rank) are shown in Figs. 3, 4, 5, where the surfaces are taken to be:

- Cube: the boundary of the set $\left\{(x, y, z) : |x| < \frac{1}{2}, |y| < \frac{1}{2}, |z| < \frac{1}{2}\right\}$;
- Sphere: $\left\{(x, y, z) : x^2 + y^2 + z^2 = 1\right\}$;
- Torus: $\left\{(x, y, z) : \left(\sqrt{x^2 + y^2} - 1\right)^2 + z^2 = \frac{1}{3}\right\}$.

The electric potentials are plot with full range in plotting areas, while the electric field strengths are limited to certain ranges due to singularity. Since the plane $z = 1/2$ coincides with the cubic surface and the electric field strength is singular, we then calculate it at slightly distance away as shown in Fig. 3d. All the calculation results agree with the theoretical concept and no fractals are found for these distributions in the given planes. While on the triangle planes for the modeled surfaces the potentials are in the exactly same value, V_s, and the field strengths are all singular.

Triangle area distribution

The minimum and maximum values of triangle areas are given in Table 1 for each polyhedron at each rank. The triangles on the initial polyhedron of cube have the same area, and each subdivision minimize the areas 4 times smaller than the original triangle, so the triangle areas on each rank of polyhedron of cube are exactly same. Figure 6 shows the edges of each triangle on initial polyhedron of triangular cube surface and its first and second subdivisions. Note that the by this subdivision way the symmetry of triangle orientation is not that of a cube, which will cause the different calculated charges in the triangles of the corners.

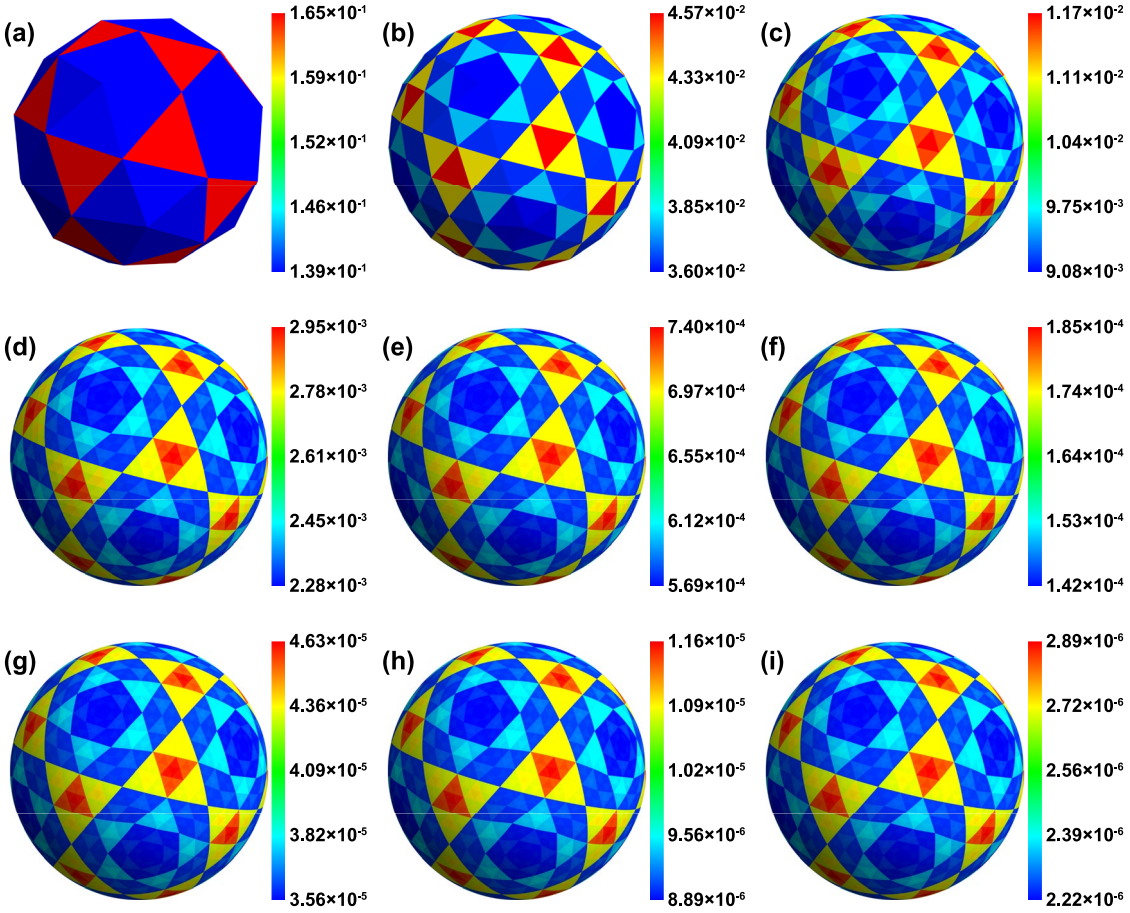

Fig. 7. The triangle area distributions for different ranks of polyhedron of sphere. (**a**–**i**) corresponds to 1st-9th rank.

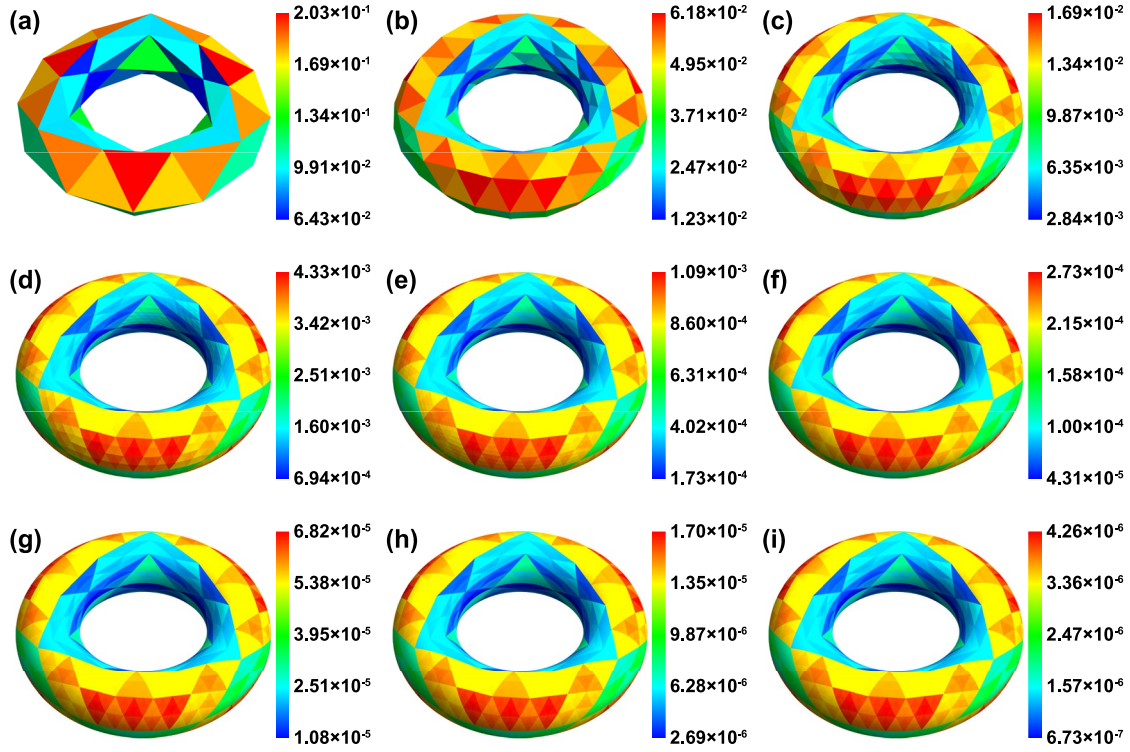

Fig. 8. The triangle area distributions for different ranks of polyhedron of torus. (**a**–**i**) corresponds to 1st-9th rank.

	Cube		Sphere		Torus	
rank	Minimum	Maximum	Minimum	Maximum	Minimum	Maximum
1	1.41×10^{-2}	2.68×10^{-2}	1.23×10^{-2}	1.32×10^{-2}	9.74×10^{-05}	1.93×10^{-02}
2	3.36×10^{-3}	9.25×10^{-3}	2.89×10^{-3}	3.61×10^{-3}	2.25×10^{-04}	5.94×10^{-03}
3	8.19×10^{-4}	3.30×10^{-3}	7.12×10^{-4}	9.34×10^{-4}	5.10×10^{-05}	1.67×10^{-03}
4	2.03×10^{-4}	1.20×10^{-3}	1.78×10^{-4}	2.35×10^{-4}	1.34×10^{-05}	4.39×10^{-04}
5	5.06×10^{-5}	4.35×10^{-4}	4.44×10^{-5}	5.89×10^{-5}	3.43×10^{-06}	1.11×10^{-04}
6	1.26×10^{-5}	1.59×10^{-4}	1.11×10^{-5}	1.47×10^{-5}	8.52×10^{-07}	2.78×10^{-05}
7	3.16×10^{-6}	5.79×10^{-5}	2.77×10^{-6}	3.68×10^{-6}	2.13×10^{-07}	6.97×10^{-06}
8	7.89×10^{-7}	2.11×10^{-5}	6.93×10^{-7}	9.21×10^{-7}	5.31×10^{-08}	1.74×10^{-06}
9	1.97×10^{-7}	7.71×10^{-6}	1.73×10^{-7}	2.30×10^{-7}	1.33×10^{-08}	4.36×10^{-07}

Table 2. The calculated minimum and the maximum values of charges by Eq. (4) among all the triangles of polyhedra of cube, sphere and torus.

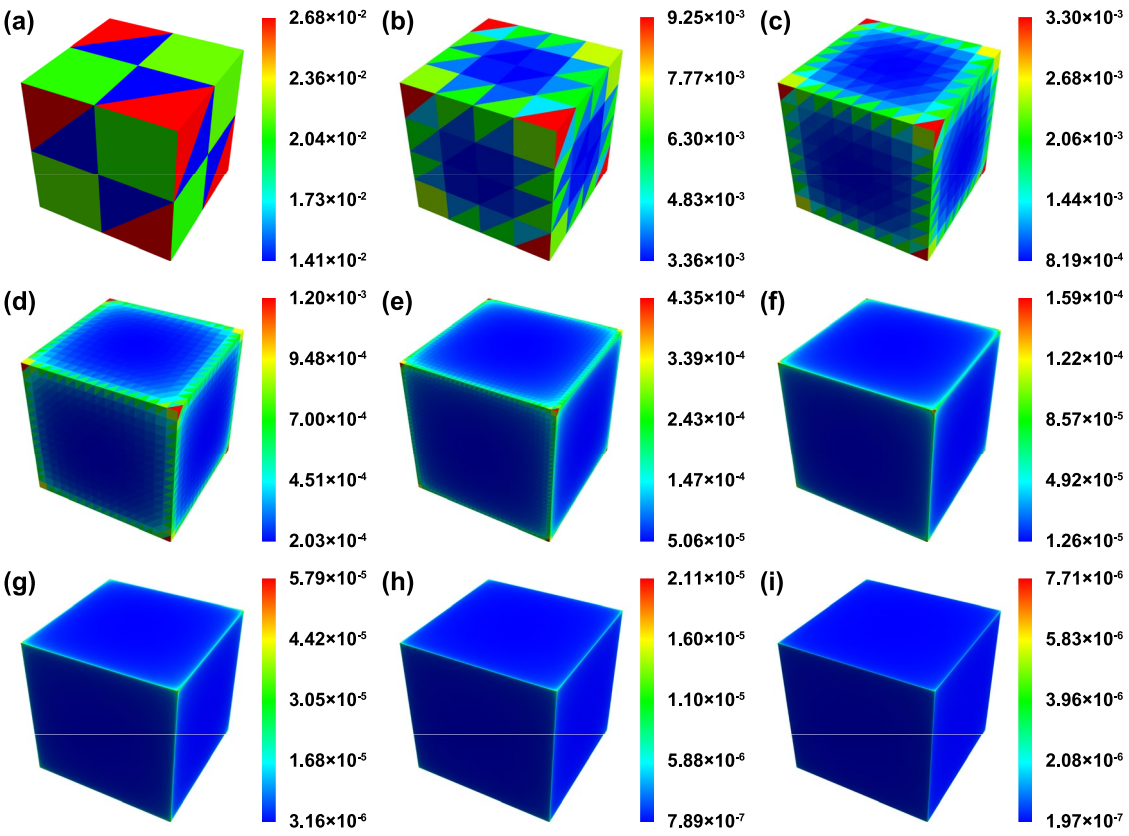

Fig. 9. The calculated charge distribution by Eq. (4) at different ranks of triangular cube surface. (**a**–**i**) corresponds to 1st-9th rank.

Subdividing a triangle on sphere or torus needs to map the new vertices to the curved surface. This step changes the subdivided triangle areas for different triangles, so the minimum and maximum triangle areas on polyhedra of sphere and torus are different. Figures 7 and 8 show the triangle area distributions for each rank of sphere and torus, respectively. This subdivision process is similar to that for obtaining the Sierpiński gasket and, therefore, the triangle area distribution becomes fractal[9].

Charge distributions

The calculated minimum and maximum values of charges on triangular surfaces by Eq. (4) are shown in Table 2 for each rank of polyhedra of cube, sphere and torus. According to these values, the charge distributions are illustrated in Figs. 9, 10, 11. Figure 9 is the charge distribution in the triangle planes of the cube surface. Since the triangle areas are the same for each triangle at any rank of the cube, this charge distribution plot is exactly the same as that of the charge density distribution plot for the cube. Note that although the triangle areas are the same for each triangle, however, the charges in these triangles are not so because the relative positions of the centroids of neighboring triangles may

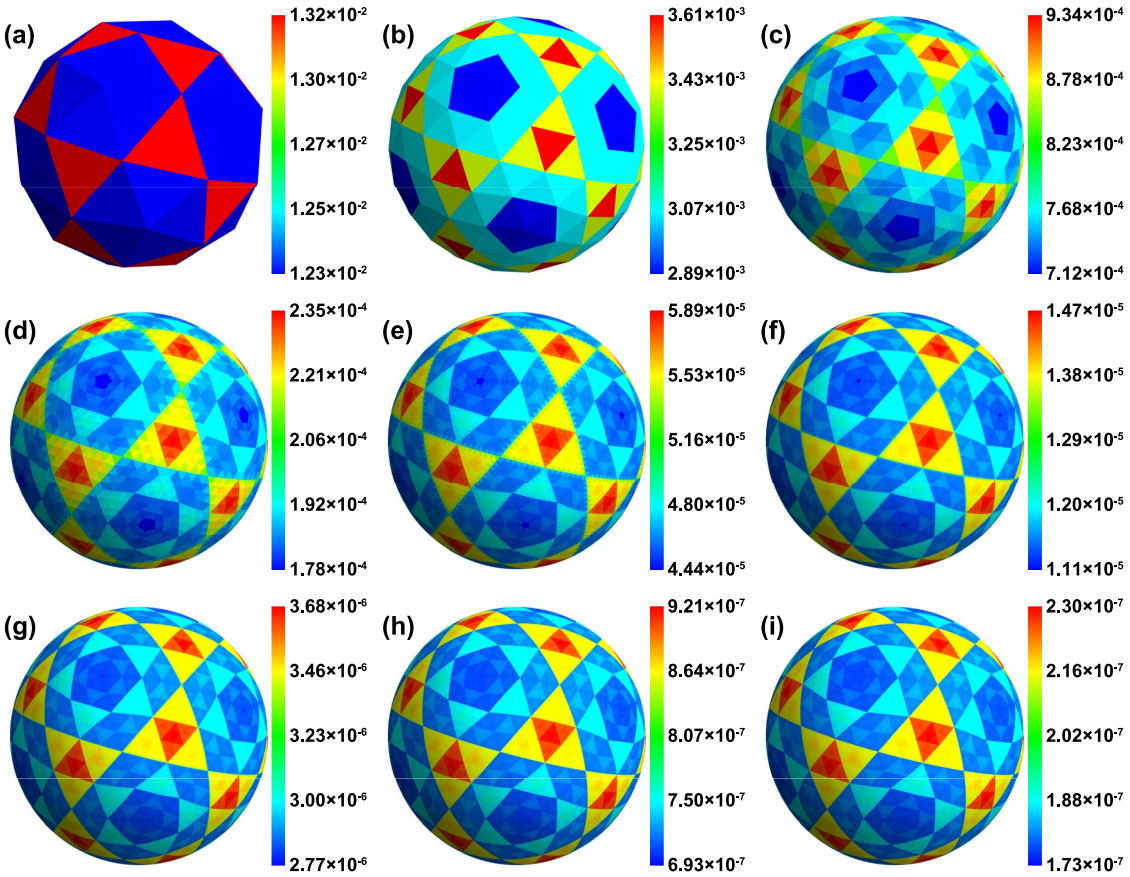

Fig. 10. The calculated charge distributions by Eq. (4) at different ranks of polyhedron of sphere. (**a**–**i**) corresponds to 1st-9th rank.

different and the calculated charges assumed to be concentrated at these centroids are changed also according to Eq. (4). Those triangles whose centroids are closer to the corners have higher charge values because theoretically more charges are distributed at corners. In addition, even for the symmetrical subdivided corner cubes their charges on the triangle planes of these corner cubes are asymmetrical as seen in Fig. 6. From the perspective of entire cube, the illustrated charge distributions also conform to the theoretical concept because charges and charge densities have higher values at corners and edges than those at the center of the cube faces. While the charge distribution is not uniform there is no fractal found on the cube surface.

But, the charge distributions on sphere and torus shown in Figs. 10 & 11 respectively, are very different from the cube case. They all form fractal patterns, which are most obviously seen for the highest rank calculated. These fractal patterns are similar to but somewhat different from the triangle area distributions (Figs. 7 & 8). It is certainly that the 3D curved surface fractal pattern also come from the way of triangle subdivision, as for the area distribution; but here the charges are derived from Eq. (4) so that the behavior of fractal intensity is different from that of area.

To quantitatively compare these behaviors, both patterns can be normalized to enable direct evaluation. Let N denote the number of triangular elements, S be the triangle area distribution, and q be the charge distribution. The normalized geometric pattern is then given by NS/A, where A is the total modeled surface area. The normalized physical pattern is Nq, under the assumption that the total surface charge is 1. These normalizations ensure that both distributions are dimensionless and consistently scaled, facilitating meaningful comparison between geometrical and physical fractal structures.

Charge density distributions

By dividing the charge value in Eq. (4) with the area of a triangle, one then obtains the charge area density distribution, which will be called simply the charge density distribution in the following. The minimum and maximum values of charge densities in the triangles are shown in Table 3 for each rank of polyhedra of cube, sphere and torus. According to Table 3, the minimum and maximum values are gradually become stable with increasing rank except for the maximum value of the cube, which represents the charge densities exactly at the vertices of the cube and should infinitely grow with the number of subdivisions. For a sphere, because it is isotropic, the ideal charge density distribution should be a constant. However, it is found that the minimum and the maximum charge density values in the triangles of polyhedra of the sphere are not the same.

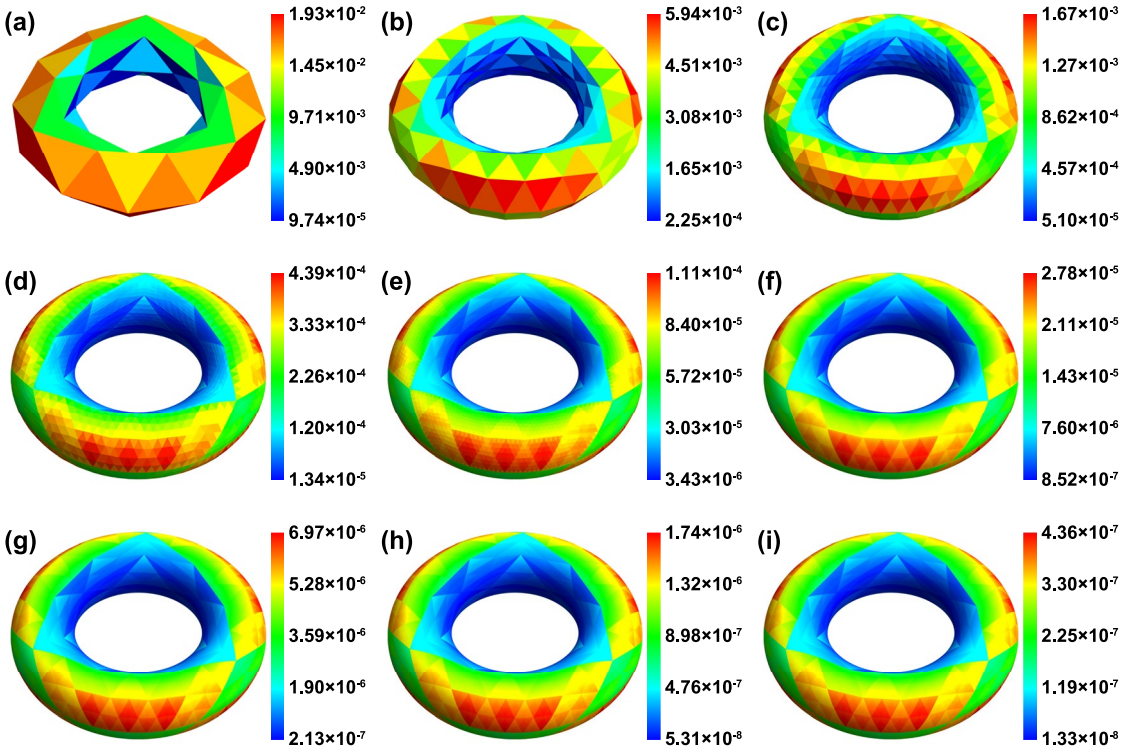

Fig. 11. The calculated charge distributions by Eq. (4) at different ranks of polyhedron of torus. (**a**–**i**) corresponds to 1st-9th rank.

	Cube		Sphere		Torus	
Ranks	Minimum	Maximum	Minimum	Maximum	Minimum	Maximum
1	0.112876	0.214188	0.080008	0.087980	0.001182	0.169316
2	0.107493	0.295874	0.078059	0.084061	0.016790	0.139554
3	0.104895	0.422954	0.076932	0.082610	0.017643	0.127666
4	0.103917	0.612585	0.076870	0.081914	0.018130	0.122396
5	0.103581	0.891685	0.076958	0.081661	0.017983	0.119883
6	0.103478	1.300391	0.077032	0.081555	0.017908	0.118647
7	0.103452	1.897736	0.077077	0.081508	0.017872	0.118033
8	0.103449	2.770144	0.077101	0.081486	0.017853	0.117726
9	0.103452	4.043925	0.077114	0.081475	0.017844	0.117573

Table 3. The calculated minimum and the maximum values of charge densities by Eq. (4) among all the triangles of polyhedra of cube, sphere and torus.

Figures 12, 13, 14 illustrate the charge density distributions derived from Eq. (4) for the cube, sphere and torus, respectively, across various subdivision ranks. Figure 12 shows the charge density distribution of the cube. Since all triangles within a given rank of the cube have equal area, this charge density distribution plot is identical to that of the charge distribution, except the contour scales are different.

In Fig. 13, especially at a high rank, it can be seen several lines across the entire sphere. These lines are exactly generated from the first subdivision in Fig. 15a. To observe more clearly the fractal pattern at high ranks one needs to change the minimum and the maximum values of contour map for the plot, as shown by Fig. 15b. Figures 15c, d demonstrate that the fractal pattern has self-similarity under magnification. The complex structure of the singular line fractal pattern is seen in Fig. 15d. The density values of the triangles on both sides of these singular lines change suddenly from nearly the minimum to nearly the maximum. Here we call them the singular lines; the reason for the existence of these singular lines is attributed to the uneven values of the triangle area distribution. Figure 13e shows the 5th order rank case and the fractal pattern for the singular lines can be seen clearly, indicating that the charge density distribution on sphere calculated with the present method forms a rather different 3D surface fractal pattern from that of the charge distribution and area distribution. The minimum and maximum values for torus also gradually become stable with increasing rank. Figure 14 shows

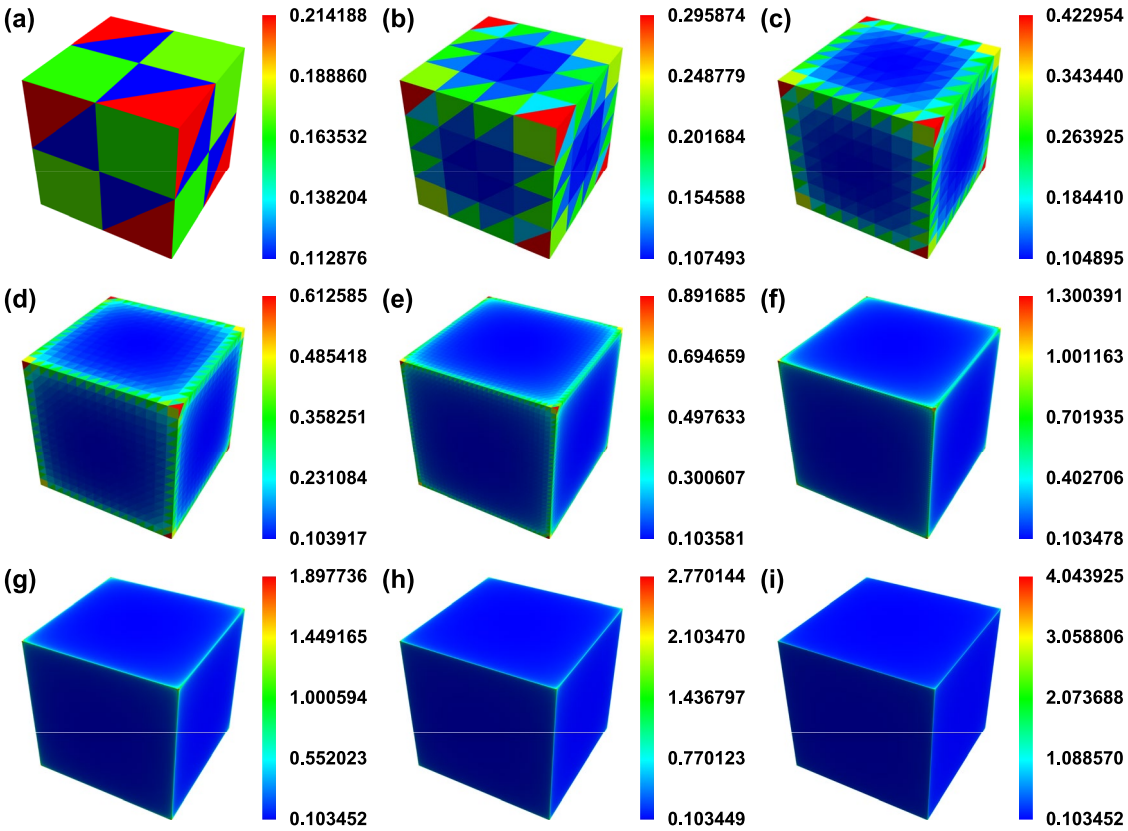

Fig. 12. The calculated charge density distribution by Eq. (4) at different ranks of triangular cube surface. (**a**–**i**) corresponds to 1st-9th rank.

that the charge density distribution is centrosymmetric and most of the charges concentrate on the outer equator instead of inner equator, which is conform to the theoretical concept. The singular lines on torus also exist at a high rank of polyhedron of torus, as more obviously seen in Fig14f. However, it is more difficult to illustrate the singular lines and fractal pattern partly due to the fact that the theoretical charge density distribution is not isotropic on torus.

Charge density distributions from analytical formula

The calculated minimum and maximum values of charge densities on triangular surfaces by analytical formula, Eq. (8), are shown in Table 4 for each rank of polyhedra of cube, sphere and torus up to 7th rank. The tendency for the changes of the minimum and maximum values with increasing rank are similar to those in Table 3. However, it can be seen that the minimum and maximum values of the sphere should quickly converge to the same value with increasing the rank. This is physically very reasonable as the charge density at an ideal sphere surface is required to be uniform. The quantitative change is very different from the results in Table 3, where due to the numerical approximation procedure the minimum and maximum values converge quite slowly.

Figures 16, 17, 18 illustrate the charge density distributions obtained from Eq. (8). One can see that the charge density distributions on cube are similar to what we obtained from Eq. (4), and those on sphere and torus have also singular lines. Comparison of Fig. 17 and Fig. 13 shows that indeed there is a small quantitative difference on the intensity between two approaches. Since the minimum and maximum values of the sphere approach to the same value by the exact solution, the singular lines do not exist on sphere when the subdivision rank $n \to \infty$ and they should not exist on torus either, representing the fact that, the fractal structure becomes weak in intensity at disappears at infinite rank. This seems to be contrary to the fractal definition. However, although self-similarity across infinite scales is mathematically required to be a fractal, considering the physical law requirement we considered in the present modelling the infinite rank cannot be physically realized because the continuity of a material will disappear down to the scale of atomic size. Therefore, the modeled fractal structure is meaningful for the mixed geometry and physics restrictions once the physical system is well above the nanoscale.

Constructed mathematical distribution

Furthermore, when we abandon the restriction to the physical quantity (like the charge density which must be uniform on pure sphere surface at infinite rank) and construct a pure mathematical quantity with the charge distribution and the area distribution, the fractal behavior can then exist up to infinite rank. For

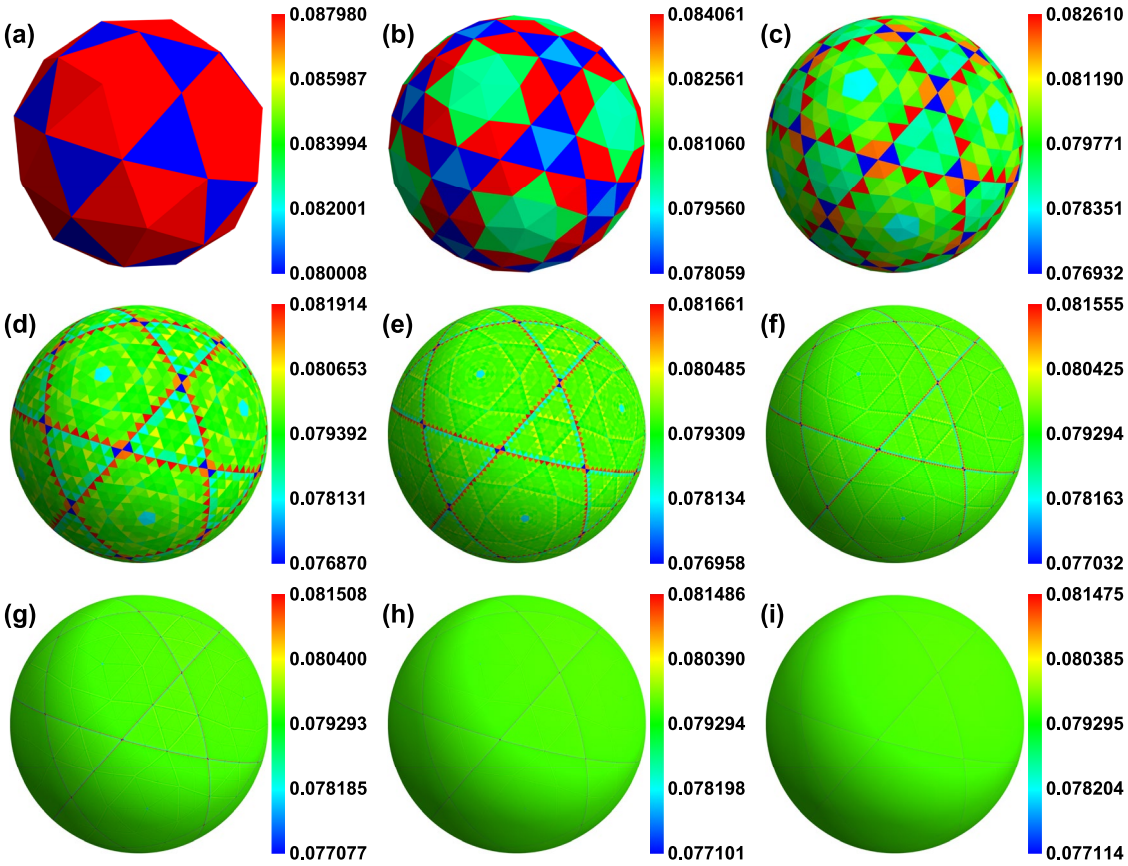

Fig. 13. The calculated charge density distributions by Eq. (4) at different ranks of polyhedron of sphere. (**a**–**i**) corresponds to 1st-9th rank.

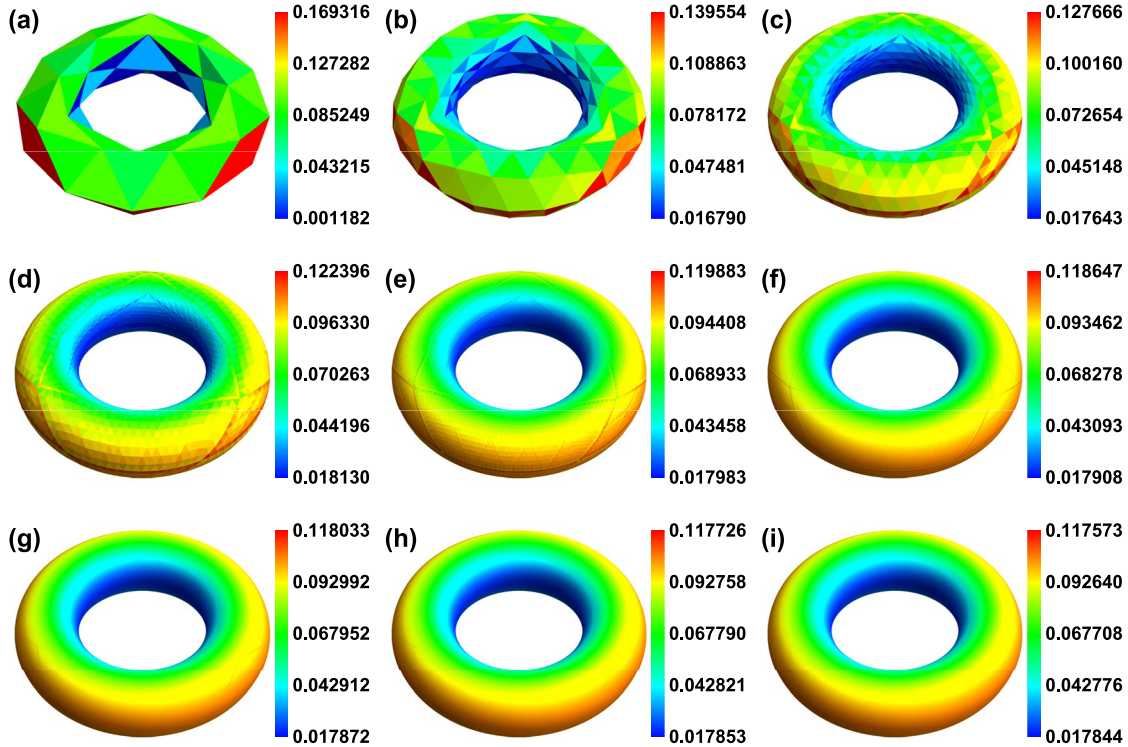

Fig. 14. The calculated charge density distributions by Eq. (4) at different ranks of polyhedron of torus. (**a**–**i**) corresponds to 1st-9th rank.

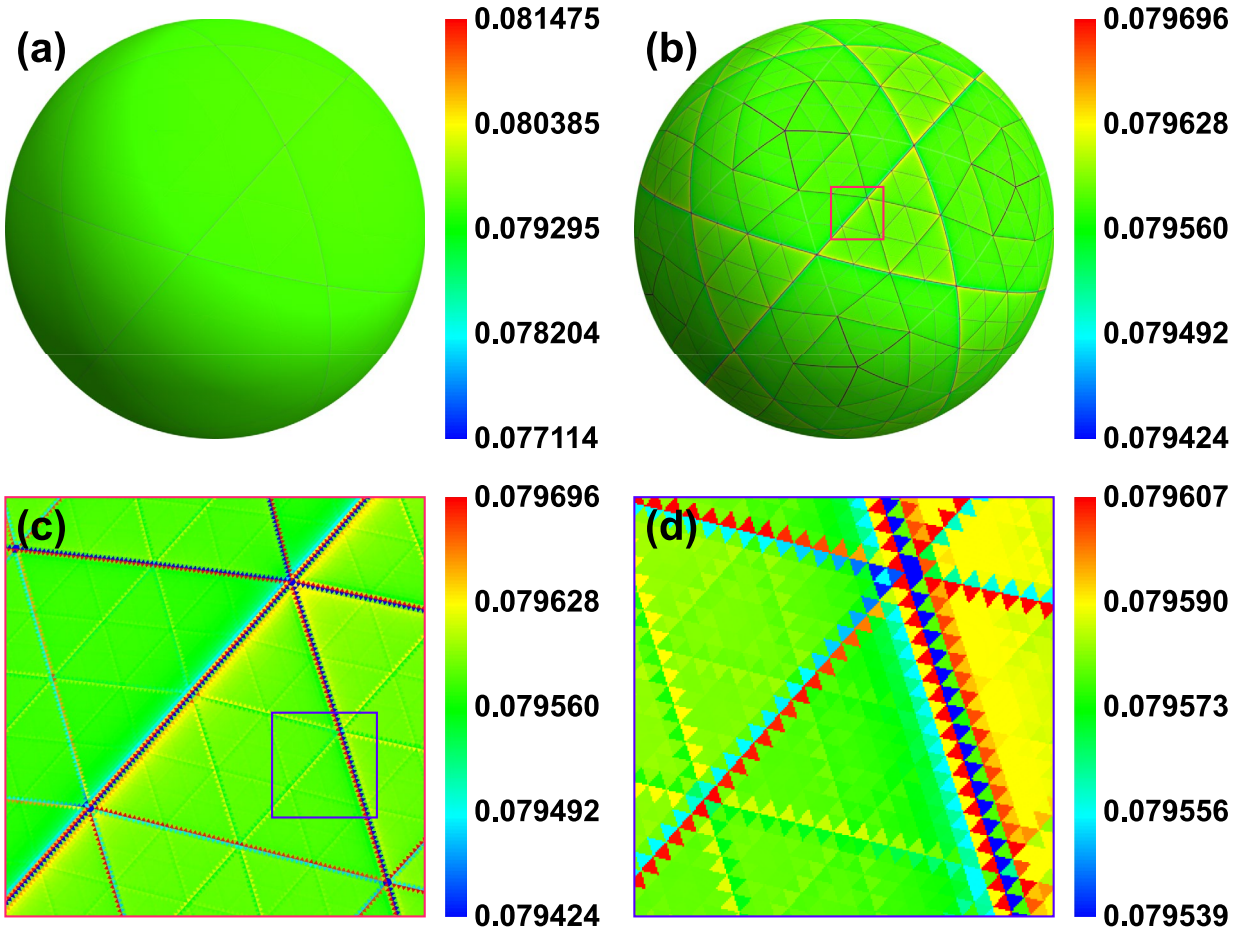

Fig. 15. The calculated charge density distributions by Eq. (4) for the 9th rank of polyhedron of sphere with different minimum and maximum values for intensity plot: (**a**) original distribution with the minimum and maximum values given in Table 3, i.e. 0.077114 and 0.081475, respectively; (**b**) minimum and maximum values are set to 0.079424 and 0.079696, respectively; (**c**) magnified region from the rectangle in (**b**); (**d**) magnified region from the rectangle in (**c**) and minimum and maximum values are set to 0.079539 and 0.079607, respectively.

example, Fig. 19 shows the product of the two differences: the area distribution minus the average triangle area, $(NS - 4\pi)\left(\sigma - (4\pi)^{-1}\right)$, where N is the number of triangles, S is the triangle area distribution and σ is the charge area density distribution obtained from Eq. (4). A very different fractal pattern structure from Fig. 7i and Fig. 10i can be observed.

Conclusion

In this work, we investigated the electrostatic charge and charge density distributions on the surfaces of isolated conductors with cubic, spherical, and toroidal geometries. Using triangular finite element meshes, we modeled the systems as they reached electrostatic equilibrium and calculated equipotential distributions that align well with theoretical expectations.

Our results reveal that on curved 3D surfaces such as the sphere and torus, the calculated charge distributions exhibit fractal-like patterns. These patterns arise from the inherent non-uniformity in triangle areas introduced through recursive subdivision. While the area distribution is purely a result of geometric operations, the charge distribution is further constrained by physical laws. Consequently, the fractal characteristics observed in these two distributions differ significantly.

Moreover, the derived charge density distribution presents a new type of fractal structure with continuous spatial intensity variation. Although the intensity range narrows with increasing subdivision rank, eventually converging toward uniformity at infinite rank, the intermediate ranks reveal rich, self-similar patterns influenced by both geometry and physics.

Ranks	Cube		Sphere		Torus	
	Minimum	Maximum	Minimum	Maximum	Minimum	Maximum
1	0.112647	0.217155	0.082511	0.086990	0.028561	0.145570
2	0.106886	0.302903	0.079821	0.082029	0.024011	0.123824
3	0.104893	0.434077	0.079251	0.080517	0.022355	0.114484
4	0.104039	0.628934	0.079295	0.079966	0.022173	0.110068
5	0.103691	0.915351	0.079406	0.079752	0.022231	0.107867
6	0.103552	1.334628	0.079484	0.079660	0.022298	0.106759
7	0.103496	1.947393	0.079529	0.079618	0.022340	0.106201

Table 4. The calculated minimum and the maximum values of charge densities by Eq. (8) among all the triangles of polyhedra of cube, sphere and torus.

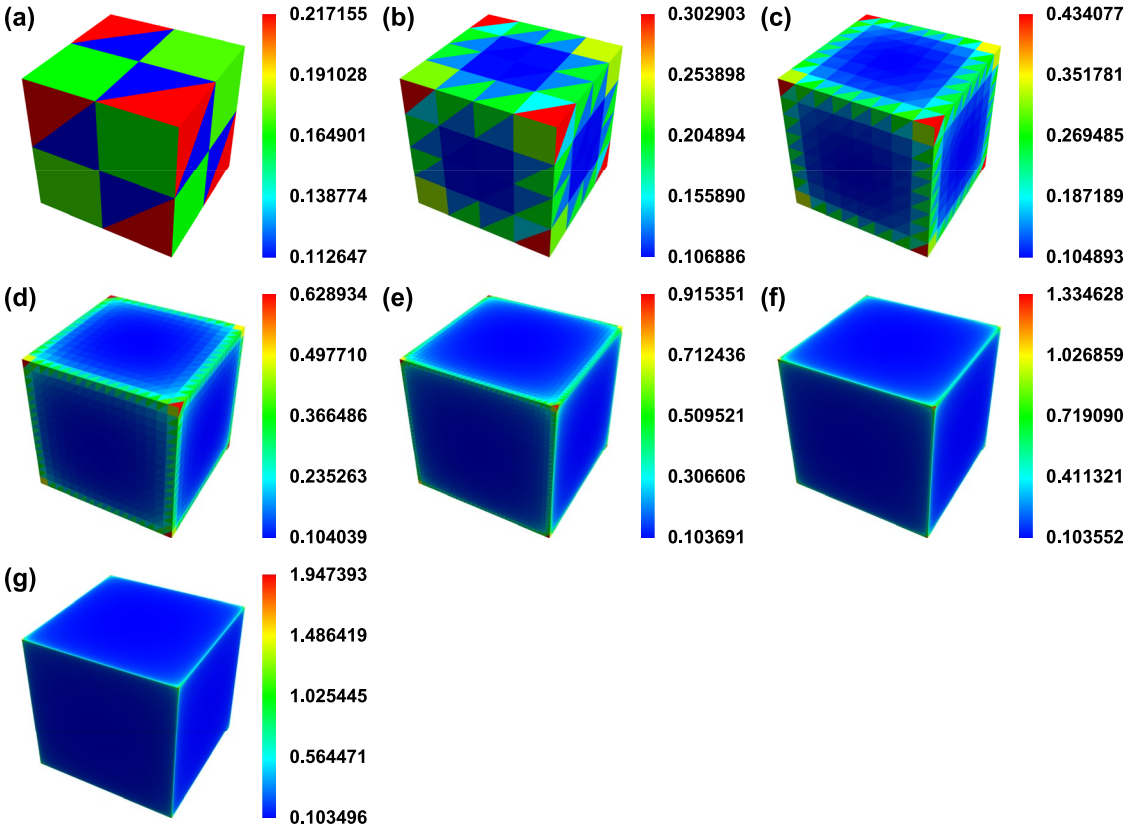

Fig. 16. The calculated charge density distributions by Eq. (8) on different ranks of triangular cube surface. (**a**–**g**) corresponds to 1st-7th rank.

This study suggests that by applying physical laws and mathematical operations to known geometrical fractals, one can generate new fractal structures with distinct properties. In addition, the work also suggests that fractal-like features observed in numerical simulations may inspire future investigations into engineered surface geometries or conductor-confinement scenarios where such effects might be measurable or useful, for example, in designing surface textures that affect field enhancement in plasmonic or nanoelectronics.

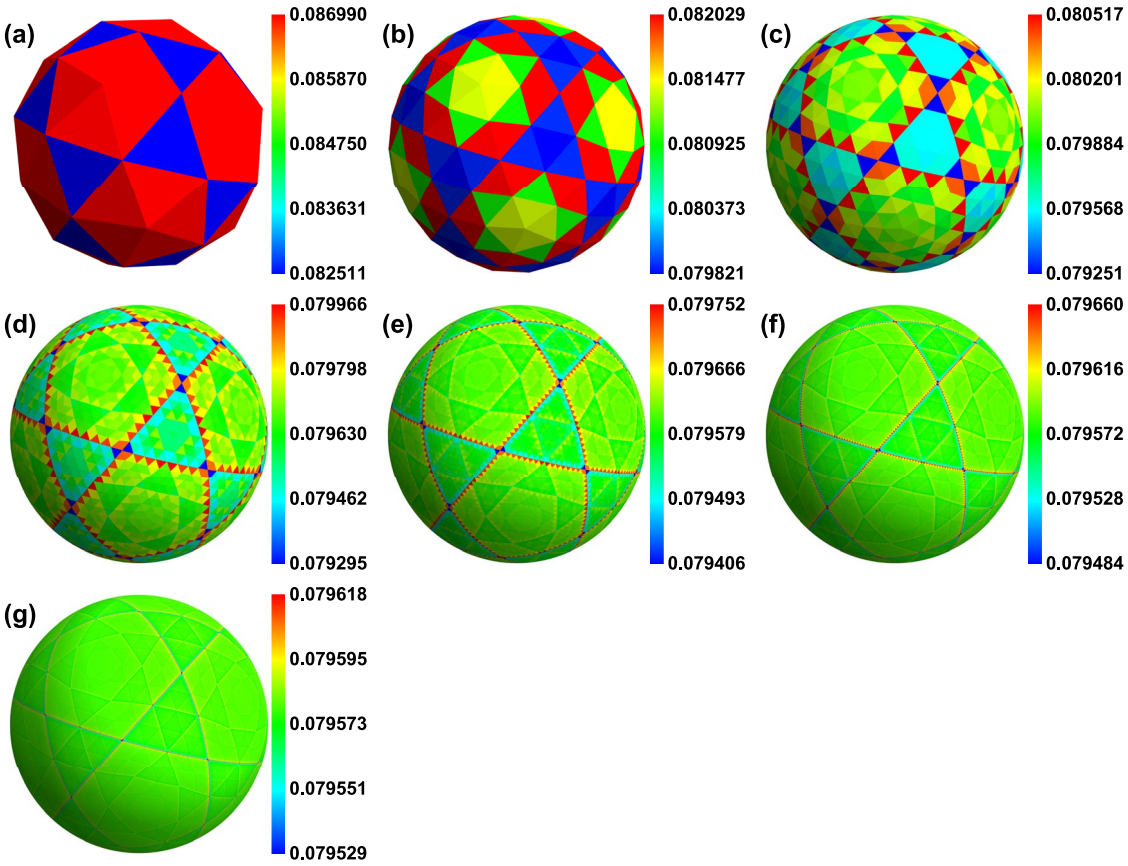

Fig. 17. The calculated charge density distributions by Eq. (8) on different ranks of polyhedron of sphere. (**a**–**g**) corresponds to 1st-7th rank.

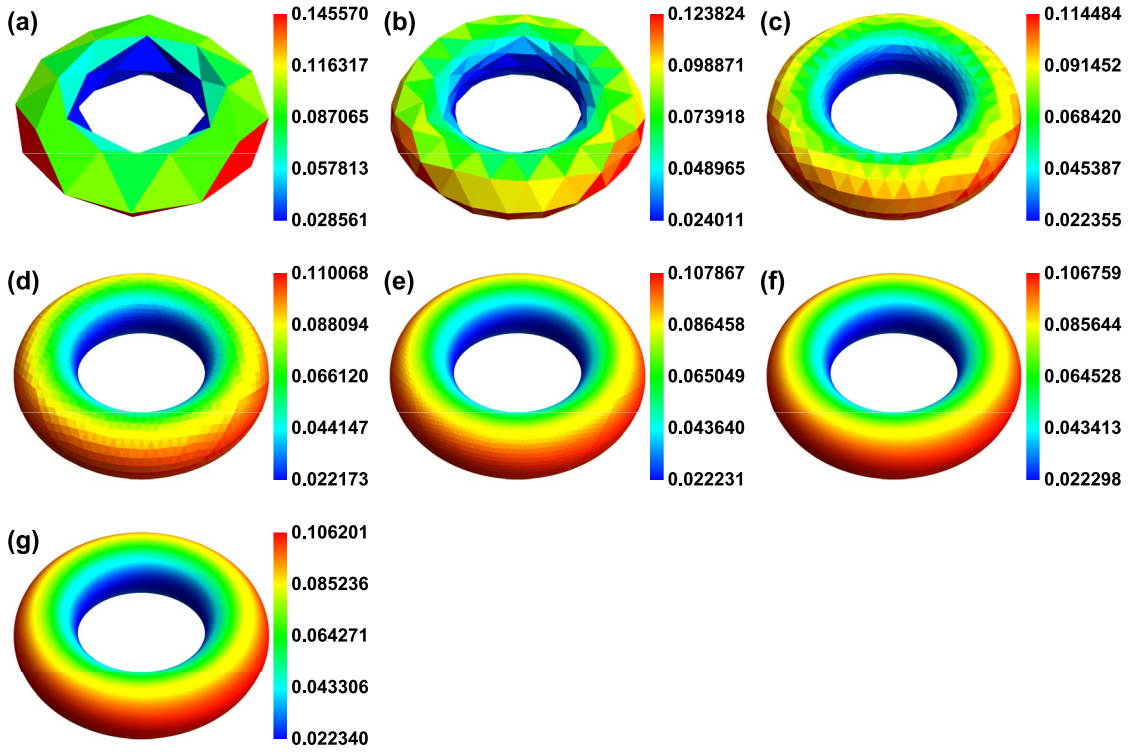

Fig. 18. The calculated charge density distributions by Eq. (8) on different ranks of polyhedron of torus. (**a**–**g**) corresponds to 1st-7th rank.

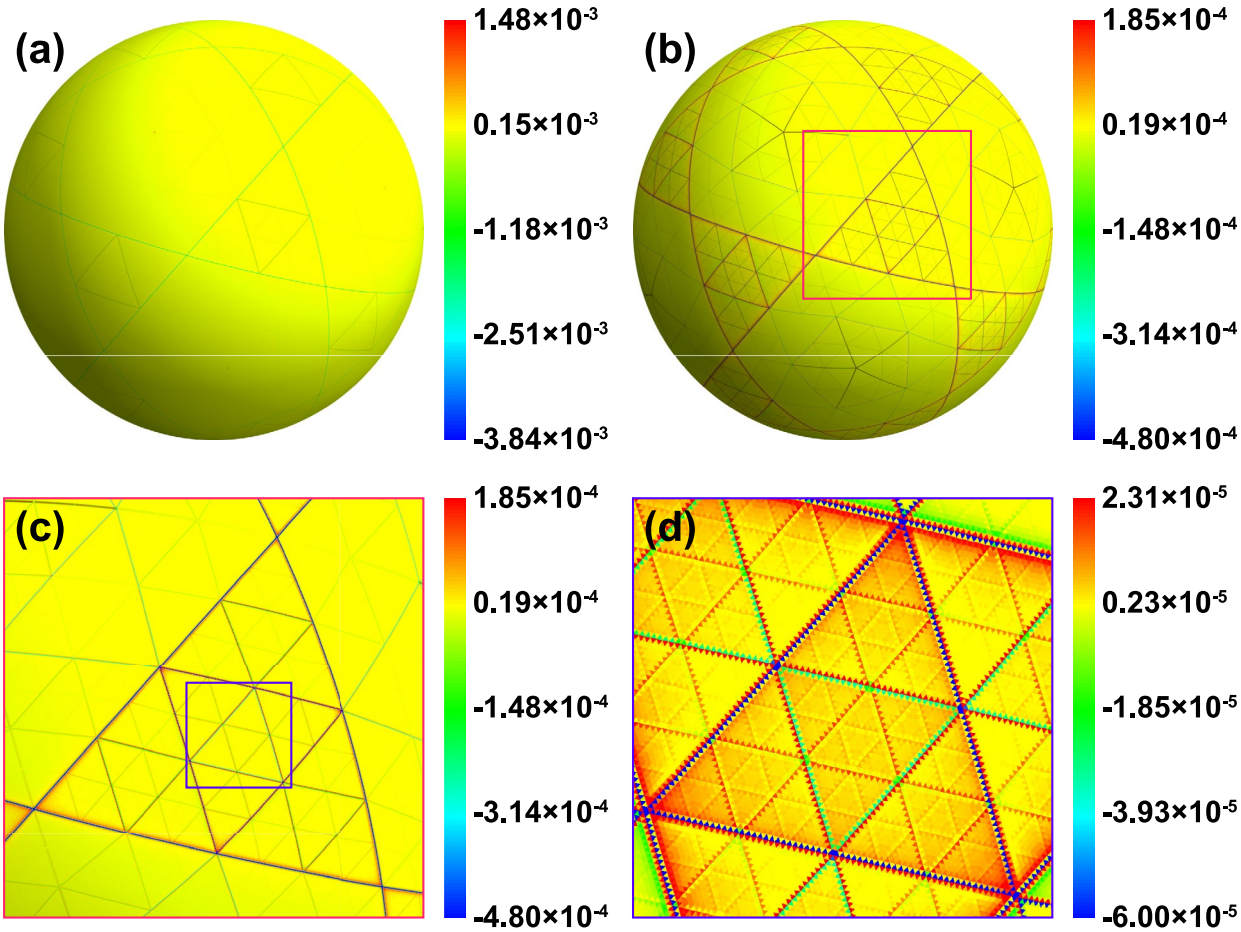

Fig. 19. The calculated fractal pattern on the 9th rank of polyhedron of sphere by formula $(NS - 4\pi) \cdot (\sigma - (4\pi)^{-1})$, where N is the number of triangles, S is the triangle area distribution and σ is the charge area density distribution obtained from Eq. (4). (**a**) full range plot with the minimum and maximum values are -3.84 × 10^{-3} and 1.48 × 10^{-3}, respectively; (**b**) minimum and maximum values are set to -4.80 × 10^{-4} and 1.85 × 10^{-4}, respectively; (**c**) magnified region from the rectangle in (**b**); (**d**) magnified region from the rectangle in (c) and minimum and maximum values are set to − 6.00 × 10^{-5} and 2.31 × 10^{-5}, respectively.

Data availability

The datasets used and/or analyzed during the current study are available from the corresponding author on reasonable request.

Received: 22 October 2024; Accepted: 16 May 2025
Published online: 31 May 2025

References

1. Mandelbrot, B. B. *The Fractal Geometry of Nature* Vol. 1 (WH freeman, 1982).
2. Mandelbrot, B. B. Fractal aspects of the iteration of z→ Λz (1-z) for complex Λ and z. *Ann. N. Y. Acad. Sci.* **357**(1), 249–259 (1980).
3. Mandelbrot, B. B. On the quadratic mapping z→ z2-μ for complex μ and z: the fractal structure of its M set, and scaling. *Physica D* **7**(1–3), 224–239 (1983).
4. Flake, G. W. *The Computational Beauty of Nature: Computer Explorations of Fractals, Chaos, Complex Systems, and Adaptation* (MIT Press, 2000).
5. Zhao, E. & Liu, D. Fractal image compression methods: A review. In *Third International Information Conference on information Technology and Applications* (ed. Zhao, E.) (IEEE, 2005).
6. Kunze, H., La Torre, D., Mendivil, F., & Vrscay, E. R. *Fractal-based Methods in Analysis*. Springer Science & Business Media. (2011).
7. Peitgen, H. O., Jürgens, H., & Saupe, D. *Fractals for the Classroom: part two: Complex Systems and Mandelbrot Set*. Springer Science & Business Media. (2012).
8. Pugh, A. *Polyhedra: A Visual Approach*. Univ of California Press. (1976).
9. White, D., Kimerling, A. J., Sahr, K. & Song, L. Comparing area and shape distortion on polyhedral-based recursive partitions of the sphere. *Int. J. Geogr. Inf. Sci.* **12**(8), 805–827 (1998).
10. Willemse, J. M., & Hawick, K. A. Generation and rendering of fractal terrains on approximated spherical surfaces. *Proc. 17th Int. Conf. Comput. Graph. Virtual Reality*. (2013).
11. Shushkevich, G. C. Electrostatic problem for a torus and a disk. *Tech. Phys.* **42**, 436–438 (1997).

12. Shushkevich, G. C. Electrostatic field of a thin, unclosed spherical shell and a torus. *Tech. Phys.* **43**, 743–748 (1998).
13. Shushkevich, G. C. Electrostatic problem for a thin, unclosed ellipsoidal shell and disk. *Tech. Phys.* **44**, 133–136 (1999).
14. Sheng, C., Junyi, L., Xin, C., Yanyi, W. & Baohua, T. Spatial potential of arbitrary uniformly charged polygons. *Eur. Phys. J. Plus* **138**(11), 1012 (2023).
15. Mebius, J. E. (2007). Derivation of the Euler-Rodrigues formula for three-dimensional rotations from the general formula for four-dimensional rotations. *arXiv preprint math/0701759*. (2007).

Acknowledgements

This work was supported in part by the National Institute for Materials Science under the support system for curiosity-driven research, JSPS KAKENHI (JP21K14656), the Kurata Grants from the Hitachi Global Foundation and from the Iketani Science & Technology Foundation. We thank Prof. H.M. Li and the supercomputing center of USTC for the support of parallel computing.

Author contributions

Haotian Chen: Writing – original draft, Investigation, Software, Methodology, Formal analysis. Bo Da: Conceptualization, Funding acquisition. Zejun Ding: Conceptualization, Writing – review & editing, Supervision, Project administration.

Declarations

Competing interests

The authors declare no competing interests.

Additional information

Supplementary Information The online version contains supplementary material available at https://doi.org/10.1038/s41598-025-02945-5.

Correspondence and requests for materials should be addressed to B.D. or Z.J.D.